BIOCHEMISTRY
including biophysical chemistry & molecular biology

Article

pubs.acs.org/biochemistry

Hidden in Plain Sight: Subtle Effects of the 8-Oxoguanine Lesion on the Structure, Dynamics, and Thermodynamics of a 15-Base Pair Oligodeoxynucleotide Duplex

Charisse M. Crenshaw,[‡] Jacqueline E. Wade,[†] Haribabu Arthanari,[§] Dominique Frueh,[∥] Benjamin F. Lane,[⊥] and Megan E. Núñez*[,†]

[†]Department of Chemistry, Mount Holyoke College, South Hadley, Massachusetts 01075, United States

[‡]Department of Molecular and Cellular Biology, Harvard University, Cambridge, Massachusetts 02138, United States

[§]Department of Biological Chemistry and Molecular Pharmacology, Harvard Medical School, Boston, Massachusetts 02115, United States

[∥]Department of Biophysics and Biophysical Chemistry, Johns Hopkins University School of Medicine, Baltimore, Maryland 21205, United States

[⊥]Charles Stark Draper Laboratory, Cambridge, Massachusetts 02139, United States

Supporting Information

ABSTRACT: The base lesion 8-oxoguanine is formed readily by oxidation of DNA, potentially leading to G → T transversion mutations. Despite the apparent similarity of 8-oxoguanine-cytosine base pairs to normal guanine-cytosine base pairs, cellular base excision repair systems effectively recognize the lesion base. Here we apply several techniques to examine a single 8-oxoguanine lesion at the center of a nonpalindromic 15-mer duplex oligonucleotide in an effort to determine what, if anything, distinguishes an 8-oxoguanine-cytosine (8oxoG-C) base pair from a normal base pair. The lesion duplex is globally almost indistinguishable from the unmodified parent duplex using circular dichroism spectroscopy and ultraviolet melting thermodynamics. The DNA mismatch-detecting photocleavage agent $Rh(bpy)_2chrysi^{3+}$ cleaves only weakly and nonspecifically, revealing that the 8oxoG-C pair is locally stable at the level of the individual base pairs. Nuclear magnetic resonance spectra are also consistent with a well-conserved B-form duplex structure. In the two-dimensional nuclear Overhauser effect spectra, base−sugar and imino−imino cross-peaks are strikingly similar between parent and lesion duplexes. Changes in chemical shift due to the 8oxoG lesion are localized to its complementary cytosine and to the 2−3 bp immediately flanking the lesion on the lesion strand. Residues further removed from the lesion are shown to be unperturbed by its presence. Notably, imino exchange experiments indicate that the 8-oxoguanine-cytosine pair is strong and stable, with an apparent equilibrium constant for opening equal to that of other internal guanine-cytosine base pairs, on the order of 10^{-6}. This collection of experiments shows that the 8-oxoguanine-cytosine base pair is incredibly stable and similar to the native pair.

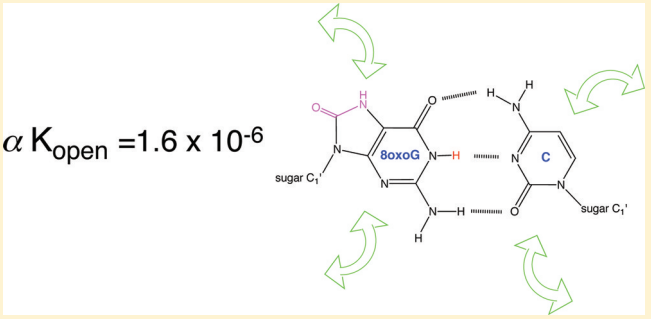

DNA is constantly being damaged by endogenous and exogenous agents.[1] Damage to the DNA bases is particularly insidious because the information content of the sequence may be lost if the base is modified; if damage is left unrepaired, covalent chemical changes to the DNA structure can lead to mutations and ultimately to cancinogenesis or apoptosis. One of the most common damage lesions in DNA is 8-oxo-7,8-dihydro-2′-deoxyguanosine (8-oxoguanine or 8oxoG), which can be readily generated by a range of oxidants and reactive species via a variety of mechanisms because of guanine's low redox potential.[2−4] If 8oxoG is not removed, the replicative DNA polymerases frequently pair 8oxoG with an incoming adenine, leading to a G to T transversion mutation.[5,6]

The 8oxoG nucleotide is chemically similar to its parent guanine. The transformation from normal base to lesion occurs via the replacement of a hydrogen at C8 with a keto group and protonation of the N7 lone pair, both at positions facing into the major groove (Figure 1 of the Supporting Information). Two consequences of the oxidation are a shift in the pK_a of imino N1 of approximately −0.7 pH unit relative to that of normal guanine and a rotation of the base dipole by 42°.[7,8] Nonetheless, the size of the base is very similar to that of the parent guanine, the lesion base remains aromatic and planar, and its Watson−Crick hydrogen-bonding edge is unchanged.[9]

Received: June 30, 2011
Revised: August 24, 2011
Published: September 8, 2011

dx.doi.org/10.1021/bi201007t | *Biochemistry* 2011, 50, 8463−8477

Both nuclear magnetic resonance (NMR)[10] and X-ray crystallographic[11] studies of the 8oxoG lesion paired with cytosine in a duplex DNA showed the B-form DNA duplex structure to be maintained. Base stacking, base pairing, and helical twist are unperturbed, even in the vicinity of the lesion. The 8oxoG stacks normally within the helix in the *anti* conformation and forms Watson−Crick hydrogen bonds to its cytosine pair. More recent structures of three duplexes containing 8oxoG, cocrystallized with a protein scaffold, show the sugar pucker to be C2′-*endo* at the lesion nucleoside consistent with canonical B-form DNA.[12] Only when paired with adenine does 8oxoG adopt the *syn* conformation to form a Hoogsteen base pair, but even in this case, the overall helical geometry is surprisingly well-conserved.[13,14]

Other data support this picture of the 8oxoG-C pair as subtle and nondisruptive with respect to the B-form DNA conformation. The substitution of 8oxoG for G in a 13-mer oligonucleotide duplex resulted in a small $\Delta\Delta G$ for the duplex−single strand equilibrium of 2.0 ± 0.7 kcal/mol.[15] This modest loss of free energy is due to a more substantial loss of enthalpy that is somewhat counterbalanced by a gain in entropy. Computational studies of 8oxoG paired with cytosine in a DNA duplex predict a variety of small changes in the structure, flexibility, and stability of the helix.[16−19]

Though DNA containing an 8oxoG-C base pair is clearly quite similar to that containing an undamaged Watson−Crick pair, multiple repair enzymes have evolved to detect and remove the lesion base from DNA, including the bacterial MutM (Fpg) glycosylase and the mammalian OGG.[20] These enzymes selectively detect relatively rare 8oxoG lesions in a sea of normal guanine bases despite the lesion's camouflaged appearance, leading to the question of how base excision repair (BER) glycosylases find their targets.[20,21] Work with uracil DNA glycosylase, another BER glycosylase, suggests that the enzyme "catches" a uracil base when it is spontaneously extruded from the helix, stabilizing the open state by slowing the rate of closing but not actively causing it to form.[22,23] Conversely, crystallographic and computational work with MutM suggests that this enzyme subtly deforms the DNA as it scans for lesions to selectively destabilize the 8oxoG lesion, catalyzing its extrusion.[24] The extent to which repair enzymes can capitalize upon inherent differences between 8oxoG and G in double-stranded DNA, as opposed to actively probing and perturbing the DNA, remains unclear. If the 8oxoG-C base pair is locally less stable than the normal G-C base pair, with distinctly different rates of base pair opening or closing or a shift in the base pair opening equilibrium toward an open state, the 8oxoG lesion might in effect signal for its own repair.

To explore further the question of whether the 8oxoG-C base pair is more destabilized and open than a normal G-C pair, we have used a variety of methods to explore sensitively its structure, thermodynamics, and base pair opening equilibrium. Our experimental DNA duplex is a nonpalindromic 15 bp oligonucleotide containing a single centrally placed lesion. The size of our construct, larger than in other structural studies, allows for examination of not only the lesion base pair and its immediate flanking bases but also several base pairs farther from the lesion. The choice of a nonpalindromic sequence, while experimentally more challenging, allows us to exclude possible cooperative effects due to two lesions in the proximity of each other. By bringing several methods to bear on the same duplex sequence for the first time, we demonstrate that the effects of 8oxoG are extremely subtle and localized to the immediate vicinity of the lesion.

MATERIALS AND METHODS

Preparation of DNA, Buffers, and the Catalyst. All DNA oligonucleotides were prepared by automated phosphoramidite synthesis, purified by PAGE or HPLC, and characterized by mass spectrometry, either in the Verdine laboratory at Harvard University or commercially (Midland Certified Reagent Co. and Integrated DNA Technologies). Residual salts were removed by purification of the DNA through Sep-Pak reverse phase cartridges (Waters Corp., Milford, MA) and extensive dialysis against 1× NMR buffer [10 mM sodium phosphate (pH 7.5) and 100 mM NaCl]. The concentration of DNA strands was determined spectrophotometrically using the following molar extinction coefficients: ε_{260} values of 139700 M^{-1} cm^{-1} for strand **1**, 133400 M^{-1} cm^{-1} for strand **1oxo**, and 144000 M^{-1} cm^{-1} for strand **2**. We annealed strands by mixing equimolar amounts of each strand to a final duplex concentration between 650 and 700 μM, heating them to 90 °C, and cooling them gradually to 4 °C. D_2O was added to the imino exchange samples to a final concentration of 5% for the purposes of the NMR lock.

Concentrated stocks of the deuterated glycine exchange catalyst were prepared at pH 7.5 to match the sample buffer pH and were added directly to the NMR tube. According to the Henderson−Hasselbach equation and an estimated pK_a of 10.2 at 8 °C, the ratio of glycine present in its active form (i.e., with a deprotonated terminal amine group) to inactive zwitterion at this pH is 1:400.

Circular Dichroism Spectropolarimetry. DNA samples were prepared at a concentration of each DNA strand of 8 μM in 1× NMR buffer. CD spectra were recorded on a Jasco J-715 spectropolarimeter at 10 °C using a 0.1 cm path length cell. Spectra were recorded between 220 and 320 nm at 0.2 nm increments with a scan rate of 20 nm/min. After subtracting the buffer blank and correcting for the molar nucleotide concentration and path length, we normalized the spectra to units of molar ellipticity to facilitate comparisons with spectra in the published literature.[25]

Spectrophotometric Measurements of DNA Melting Thermodynamics. We annealed DNA duplexes to a concentration of 0.8−21 μM in 1× NMR buffer by heating them to 80 °C and cooling them gradually to 4 °C. Samples were degassed at 4 °C to prevent formation of bubbles and were placed in cuvettes with a path length appropriate to give an absorbance at 260 nm of approximately 0.5 (0.1, 0.2, 0.5, or 1 cm). The absorbance at 260 nm was measured as a function of temperature in a Varian Cary 50 UV−visible spectrophotometer with a Peltier temperature-controlled cell. The absorbance was measured every 0.1 min, while the temperature was ramped upward at a rate of 0.5 °C/min between 8 and 80 °C. The melting temperature (T_m), defined here as the inflection point of the temperature versus absorbance curve, was determined from the first derivative. At least three independent measurements were made at each of the five concentrations for each duplex.

The T_m values and concentrations were used to determine the change in enthalpy and entropy for the formation for each duplex using a form of the van't Hoff equation:

$$\frac{1}{T_m} = \frac{R(\ln C_{tot})}{\Delta H} + \frac{\Delta S - 1.39R}{\Delta H} \quad (1)$$

where C_{tot} is the total concentration of DNA strands, which is twice the duplex concentration. A plot of $1/T_m$ versus ln C_{tot} is a straight line whose slope and intercept are used to determine the change in enthalpy and entropy associated with duplex formation. The change in Gibbs free energy associated with duplex formation was calculated from the change in enthalpy and entropy at 25 °C.

Cleavage of DNA Using Rh(bpy)$_2$(chrysi)$^{3+}$. DNA samples were annealed to a duplex concentration of 8 μM with trace amounts of DNA containing a ^{32}P-labeled phosphate at the 5′ end. Experimental samples contained either 5 or 10 μM Rh(bpy)$_2$(chrysi)$^{3+}$ as described in the legend of Figure 2. Dark control samples contained 10 μM rhodium complex, and light control samples contained no Rh(bpy)$_2$(chrysi)$^{3+}$. All samples except the dark controls were irradiated simultaneously in closed 1.7 mL plastic microcentrifuge tubes placed directly on top of a visible light box for 10 h. After being irradiated, samples were dried under vacuum in the dark, resuspended in denaturing running dye, heated briefly on a heat block at 90 °C, and loaded directly onto a preheated 18% denaturing polyacrylamide gel.[26] The location of cleavage was confirmed by comparison to Maxam−Gilbert purine-specific reaction controls (not shown). Gels were digitized by phosphorimagery on a Molecular Dynamics Storm 820 system (Amersham Biosciences), and band intensities were analyzed in ImageQuant.

One-Dimensional (1D) and Two-Dimensional (2D) NMR Spectra. 1D ^{1}H spectra were recorded at Harvard University on a Bruker AVANCE 700 MHz NMR instrument equipped with a 5 mM CPTCI cryogenic probe. Water suppression was achieved using DANTE-based excitation sculpting with a W5 block.[27] 1D spectra were recorded at 8 °C on samples containing either no catalyst (duplex **1**−**2**) or 0.0125 mM catalyst (duplex **oxo1**−**2**).

2D NOESY[28,29] experiments were performed at Harvard Medical School on a Bruker 750 MHz NMR instrument equipped with a triple-resonance TXI cryogenic probe. Two spectra were recorded for each sample. In both cases, the mixing time was 250 ms. The first NOESY spectrum was recorded in a 95% H_2O/5% D_2O mixture at 10 °C. The spectral dimensions were 20 ppm (^{1}H, 2048 complex points) by 10 ppm (^{1}H, 500 complex points); 64 scans were gethered with a recycling delay of 1 s. A second spectrum was recorded in 100% D_2O at 25 °C. The spectral dimensions were 10 ppm (^{1}H, 2048 complex points) by 10 ppm (^{1}H, 600 complex points); 32 scans were gathered with a recycling delay of 1 s. Spectra were processed with NMRPipe.[30] They were superimposed, their resonances assigned, and their chemical shifts measured in Sparky[31] according to the NOE walk method.[32−34] In the absence of COSY experiments, H4′ and H5′ protons were not assigned. A model of duplex **1**−**2** was created using Nucleic Acid Builder written by the Case group at Rutgers University.[35] The model was utilized in iMol without further refinement or structural modification purely for the purposes of visualization.

Measurement of Base Pair Opening by NMR. To monitor the exchange of imino protons and by extension to quantify base pair opening, we used magnetization inversion transfer from water protons as described by Guéron and Leroy.[36] Imino exchange experiments were performed on a Bruker AVANCE 700 MHz NMR instrument with a 5 mM CPTCI cryogenic probe at Harvard University or on a Bruker 600 MHz NMR instrument with a TCI cryogenic probe at the University of Massachusetts (Amherst, MA). In short, inversion of the water proton magnetization was accomplished via a DANTE pulse scheme, magnetization transfer occurred during a mixing time (t_{mix}), and a jump-and-return sequence was used to suppress the water resonance.[37,38] Gradients were also included in the pulse sequence to suppress the transverse components of the solvent magnetization and reduce radiation damping.[36] All spectra were recorded at 8 °C, and the temperature was calibrated before each run using the chemical shifts of a methanol standard.[39,40]

To measure the exchange rate of the imino protons, we first defined the parameters for water inversion and relaxation for each combination of sample and instrument. The efficiency of water inversion (E) was determined by integrating the area under the water peak for samples with and without a DANTE inversion (W_{inv} and W_{eq}, respectively):

$$E = 1 - \frac{W_{inv}}{W_{eq}} \quad (2)$$

where E, determined independently for each data set, was always between 1.90 and 2.00. An apparent longitudinal relaxation rate for water ($R_{1w} = 1/T_{1w}$) was measured by inversion recovery with the same pulse sequence used for the imino exchange measurements, in which the jump-and-return sequence was replaced by an excitation pulse. This ensured that the resulting water relaxation rate described the behavior of water during the imino exchange experiment and accounted for the DANTE inversion and gradients. The water signal intensity W_z was then measured as a function of t_{mix}:

$$W_z(t_{mix}) = W_{z,eq}(1 - Ee^{-t_{mix}R_{1w}}) \quad (3)$$

Fourteen spectra were obtained with mixing times ranging between 1.2 ms and 15 s (Table 1 of the Supporting Information). The water relaxation curve was not exactly exponential because of residual radiation damping, so the nonlinear least-squares fit value of R_{1w} was determined independently for each sample and instrument between 1.2 ms and 2 s to match the time window sampled in the exchange experiment. R_{1w} was equal to 0.15−0.16 on the 700 MHz spectrometer and 0.30−0.40 on the 600 MHz spectrometer.

Imino exchange rates were obtained by magnetization inversion transfer at 22 different mixing times between 520 μs and 2 s (Table 2 of the Supporting Information). The NMRPipe suite of programs[30] was used to uniformly zero fill, Fourier transform, phase, crop, and apply a first-order baseline to each group of 22 spectra, as well as to establish the approximate chemical shift of each peak. Matlab (MathWorks, Natick, MA) was used to deconvolute overlapping peaks in the spectrum and determine exchange and relaxation times. First, spectra were aligned by cross correlation along the chemical shift axis, and the height of each peak was determined at each time point. The peak heights as a function of time were used to estimate the exchange rate for each imino peak (k_{ex}) by nonlinear least-squares fitting to eq 4:

$$\frac{I_z(t_{mix})}{I_{z,eq}} = 1 + Ek_{ex}(e^{-R_{1i}t_{mix}} - e^{-R_{1w}t_{mix}}) \quad (4)$$

where E and R_{1w} were determined as described above, $I_z(t_{mix})$ and $I_{z,eq}$ were the measured intensities of the imino peaks after

time t_{mix} and at equilibrium, respectively. The exchange rate k_{ex} and R_{1i} (which represents a combination of the imino proton relaxation rate and the chemical exchange rate k_{ex}) were determined by fitting eq 4 to the data. To refine parameter estimates for overlapping peaks, these values of k_{ex} and R_{1i} were then used to seed a multiparameter nonlinear least-squares fit of a set of Lorentzian peaks to all 22 spectra simultaneously. The fit was implemented in Matlab using the *nlinfit* function. Each of the peaks was modeled using five free parameters [chemical shift, line width, intensity (volume), R_{1i}, and k_{ex}].

Over a wide range of catalyst concentrations, the relationship between the rate of exchange (k_{ex}) and the catalyst concentration ([B]) can be described by

$$\frac{1}{k_{ex}} = \tau_{ex} = \frac{1}{k_{op}} + \frac{k_{cl}}{\alpha k_{op}(k_B[B] + k_{int})} \quad (5)$$

where k_{int} is the uncatalyzed intrinsic rate of exchange of the imino proton and α is a constant that reflects the accessibility of the imino proton to the catalyst (probably ~0.1 for glycine).[22,41] k_{op} and k_{cl} are the rate of base pair opening and closing, respectively. The ratio between k_{op} and k_{cl} gives the apparent equilibrium constant for base pair opening

$$\alpha K_{op} = \frac{k_{op}}{k_{cl}} \quad (6)$$

k_B is a second-order rate constant for base catalysis, a constant that can be directly calculated for each type of imino proton:

$$k_B = \frac{k_D}{1 + 10^{pK_a^{nu} - pK_a^B}} \quad (7)$$

With a biomolecular collision rate k_D approximately equal to 0.47×10^9 M^{-1} s^{-1}, the k_B of DNA nucleotides in glycine buffer was calculated to be 3.1×10^8 M^{-1} s^{-1} for thymine, 3.9×10^8 M^{-1} s^{-1} for guanine, and 4.5×10^8 M^{-1} s^{-1} for 8oxoG (the latter based on an assumed pK_a 0.70 pH unit lower than that of G at the same temperature).[7,36]

According to eq 5, a plot of the inverse of the base concentration versus the inverse of the exchange rate gives a curve such that at low concentrations, the measured rate of exchange reflects the intrinsic rate of exchange (k_{int}) of the imino proton by other weak bases in its environment (most likely its complementary nucleotide and surrounding nucleotides); at infinitely high concentrations, the rate of exchange approaches the rate of opening (k_{op}). At very low catalyst concentrations similar to those used here, the apparent equilibrium constant for base pair opening (αK_{op}) and the intrinsic rate of exchange (k_{int}) can be determined from a plot of k_{ex} versus [B] according to the following simplified linear relationship as described by Every and Russu:[42]

$$k_{ex} = \alpha K_{op}(k_{int} + k_B[B]) \quad (8)$$

The exchange data between 5 and 600 mM glycine were fit to this equation in Gnuplot to give best-fit values of k_{int} and αK_{op} together with their associated uncertainties.

RESULTS

The 15-mer DNA duplexes used in these studies are listed in Table 1. Duplex **1**−**2** (the undamaged control parent duplex) and duplex **1oxo**−**2** are identical except for the presence of the 8oxoG lesion at position 8. Unlike the duplexes used in the original NMR and X-ray structural studies of 8oxoG-C in DNA,[10,11] this sequence is not palindromic and contains a single lesion, allowing us to examine longer-range effects on the 7 bp flanking the lesion on either side.

Table 1. Sequences of the 15 bp DNA Oligonucleotide Duplexes[a]

Parent Duplex ***1-2***	
Strand 1	5'- C_1 C_2 A_3 T_4 C_5 G_6 A_7 **G_8** A_9 C_{10} T_{11} G_{12} T_{13} G_{14} C_{15} -3'
Strand 2	3'- G_{30} G_{29} T_{28} A_{27} G_{26} C_{25} T_{24} C_{23} T_{22} G_{21} A_{20} C_{19} A_{18} C_{17} G_{16} -5'
Lesion Duplex ***1oxo-2***	
Strand 1oxo	5'- C_1 C_2 A_3 T_4 C_5 G_6 A_7 **oG** A_9 C_{10} T_{11} G_{12} T_{13} G_{14} C_{15} -3'
Strand 2	3'- G_{30} G_{29} T_{28} A_{27} G_{26} C_{25} T_{24} C_{23} T_{22} G_{21} A_{20} C_{19} A_{18} C_{17} G_{16} -5'

[a]Nucleotides are numbered sequentially from the 5′ end of each strand, indicated with subscripts. The location of the 8-oxoguanine lesion, fortuitously at position 8, is designated oG.

Effect of the 8oxoG Lesion on Duplex Stability, Global Structure, and Thermodynamics. We used three established techniques to confirm the formation of stable, B-form double helices by strands **1** and **2** (parent duplex) and **1oxo** and **2** (lesion duplex) and to assess the similarity between the two duplexes: circular dichroism spectropolarimetry (CD), UV melting thermodynamic measurements, and cleavage by $Rh(bpy)_2(chrysi)^{3+}$.

The circular dichroism spectra of both parent and lesion duplexes have maxima around 275 nm, minima around 248 nm, and a crossover point around 261 nm, consistent with the 15-mer oligonucleotides forming a B-form DNA double helix (Figure 1A).[43−45] Both spectra are distinctly different from a single-stranded control but are almost identical to one another between 220 and 320 nm.

The UV melting curves for the parent and lesion duplexes are also quite similar to one another, both in shape and in inflection point, though the lesion duplex shows a more gradual premelting transition (Figure 2 of the Supporting Information). Generally, the 8oxoG lesion causes the melting temperature (T_m) of this 15-mer duplex to decrease by only ~1 °C at any given concentration. When these measured T_m values are plotted as a function of duplex concentration (Figure 1B), the thermodynamic parameters ΔH, ΔS, and ΔG can be determined using the van't Hoff relationship (eq 1). In this 15-mer duplex, the change in the free energy of duplex formation due to the 8oxoG lesion ($\Delta\Delta G$) is 0.4 ± 1.1 kcal/mol (Figure 1C and Table 3 of the Supporting Information).

$Rh(bpy)_2(chrysi)^{3+}$ is a water-soluble, cationic transition metal complex that has been shown to bind selectively by insertion of its large chrysi ligand into destabilized regions of the DNA double helix, in particular to base mismatches, and to cleave the DNA backbone at these sites upon photoexcitation with visible light.[46,47] When incubated and photoirradiated with parent duplex **1**−**2**, the complex cleaves quite weakly, i.e., ~1% of strands after irradiation for 10 h on a visible light box (Figure 2). Cleavage in the parent duplex occurs predominantly at pyrimidines, specifically C_5 and somewhat less at C_{10} and T_{11} on primary strand **1** and at C_{23} and C_{25} on complementary strand **2** (lanes 1 and 2 and lanes 9 and 10, respectively). This cleavage is both rhodium- and light-dependent, as it does not occur in either the light or dark control lanes (lanes 3, 4, 11, and 12). Interestingly, the pattern of cleavage does not change with the substitution of 8oxoG at position 8 of strand **1** (lanes 5, 6, 13, and 14). The intensity of photocleavage increases quite modestly at C_{23} and C_5 in the 8oxoG duplex (~20−40%), while cleavage at C_{25} remains relatively unchanged. Replacement of

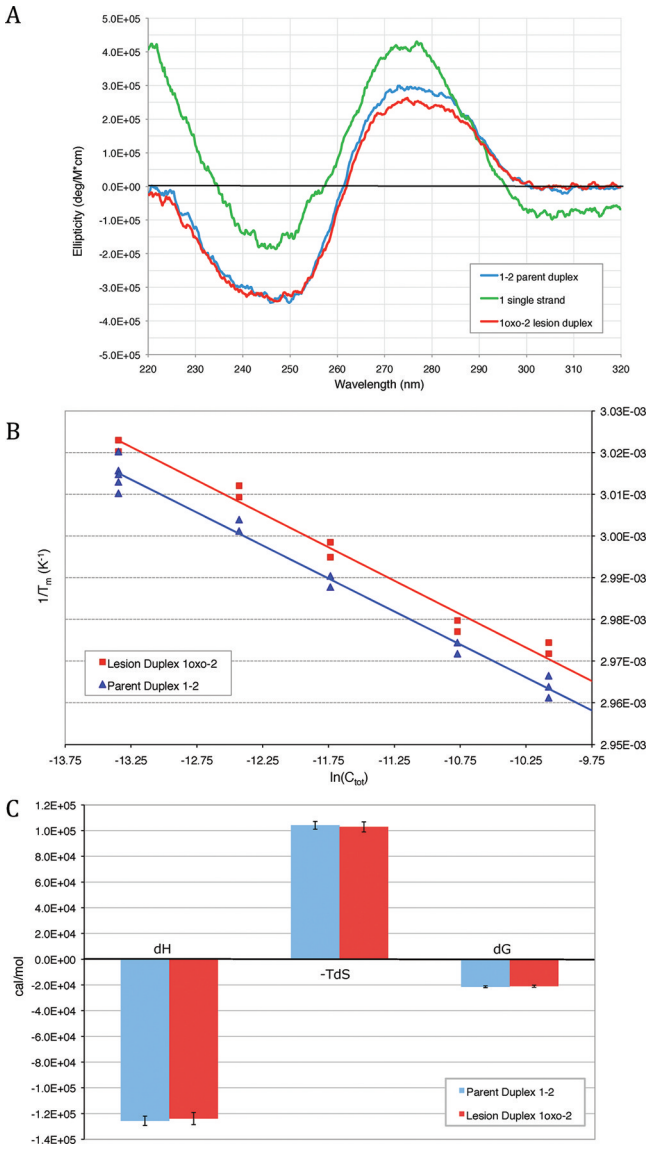

Figure 1. Circular dichroism spectrum and UV melting thermodynamics. (A) CD spectrum of parent duplex **1**−**2**, lesion duplex **1oxo-2**, and single-stranded **1** in sodium phosphate buffer at 10 °C. Each strand was present at a concentration of 8 μM. The shapes of the parent **1**−**2** and lesion **1oxo**−**2** duplex spectra (blue and red, respectively) are similar to each other and also consistent with previously published spectra for B-form DNA double helices. (B) van't Hoff plot of the relationship between duplex concentration and melting temperature for parent duplex **1**−**2** (blue) and lesion duplex **1oxo**−**2** (red), as described by eq 1. (C) Comparison of the thermodynamic parameters ΔH, $-T\Delta S$, and ΔG for formation of the parent (blue) and lesion (red) duplexes at 298 K.

C_{23} with an adenine in strand **2** to create a G-A or 8oxoG-A mispair at position 8 (lanes 17−24) does not increase the extent of chrysi photocleavage appreciably at this site, at least not on the primary strand.

Effect of the 8oxoG Lesion on Duplex Structure. Two-dimensional nuclear Overhauser effect spectroscopy (NOESY) was also utilized to evaluate the effect of the 8oxoG lesion on duplex structure. Because of the ordered and highly predictable structure of the double-stranded DNA polymer, most of the DNA duplex protons in a NOESY spectrum can be routinely assigned without additional spectra or specific labels.[32−34] By

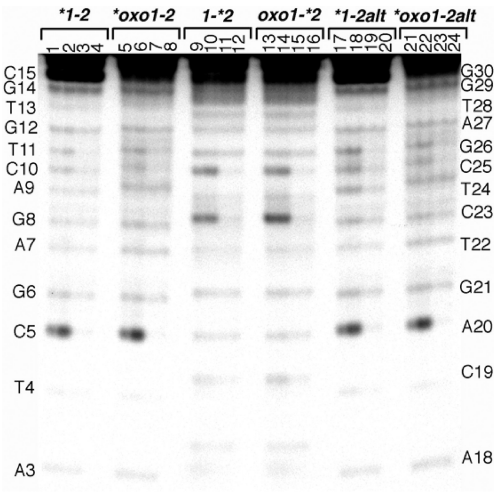

Figure 2. Probing duplex stability with $Rh(bpy)_2(chrysi)^{3+}$. DNA duplexes were incubated with $Rh(bpy)_2(chrysi)^{3+}$ for 10 h on a visible light box at room temperature to detect destabilized base pairs. The samples were loaded identically in each group of four lanes: lanes 1, 5, 9, 13, 17, and 21, 5 μM chrysi and $h\nu$; lanes 2, 6, 10, 18, and 22, 10 μM chrysi and $h\nu$; lanes 3, 7, 11, 15, 19, and 23, light control (with $h\nu$ but no chrysi); lanes 4, 8, 12, 16, 20, and 24, dark control (10 μM chrysi but no $h\nu$). Asterisks indicate the strand that is radiolabeled with ^{32}P on its 5′ end. The first two groups of lanes compare cleavage in the parent vs the lesion duplex labeled on primary strand **1** or **1oxo**; the central two groups compare cleavage on duplexes with complementary strand **2** labeled, and the last two groups compare cleavage on duplexes with the labeled primary strand annealed with an alternative complementary strand containing an adenine at position 23, creating a G_8A_{23} or $oxoG_8A_{23}$ mispair. The sequence of primary strand **1** is shown for comparison at the left side of the gel and that of strand **2** on the right side. Note that the darkest bands represent <1% of the total lane, consistent with a low level of binding and cleavage to stable, well-matched DNA duplexes.

"walking" down each strand consecutively and using a general knowledge of DNA structure, we could assign the H1′, H2′, and H2″ sugar protons as well as most of the base protons (aromatic, imino, cytosine amino, and thymine methyl) and those H3′ protons that were not overwhelmed by the water resonance.

The NOESY spectra of the 8oxoG lesion duplex were assigned using this series of NOE walks and known interatomic distances. In the region of the spectrum containing cross-peaks between the sugar H1′/cytosine H5 and H2/H6/H8 aromatic protons, as well as in the region containing cross-peaks between the sugar H2′/H2″ and H2/H6/H8 aromatic protons, the connectivity is interrupted around the 8oxoG lesion base itself because its H8 aromatic proton has been replaced with a keto group. On the complementary strand, the walk continues past the lesion uninterrupted (Figures 3 and 4 of the Supporting Information), which confirms that the 8oxoG lesion duplex forms a fully annealed and stable B-form helix. The imino−imino walk from base to base down the center of the helix is also not interrupted by the presence of the lesion, indicating that base pairing is intact along the entire helix (Figure 3a,b).

Because the 8oxoG lesion does not perturb the global B-form conformation, it is more informative to directly compare the parent and lesion duplexes. By assigning peaks in both the parent duplex and the 8oxoG duplex spectra and overlaying the two, we could evaluate the overall effect of the lesion on duplex structure in both specific location and magnitude. Critically, the

dx.doi.org/10.1021/bi201007t | Biochemistry 2011, 50, 8463−8477

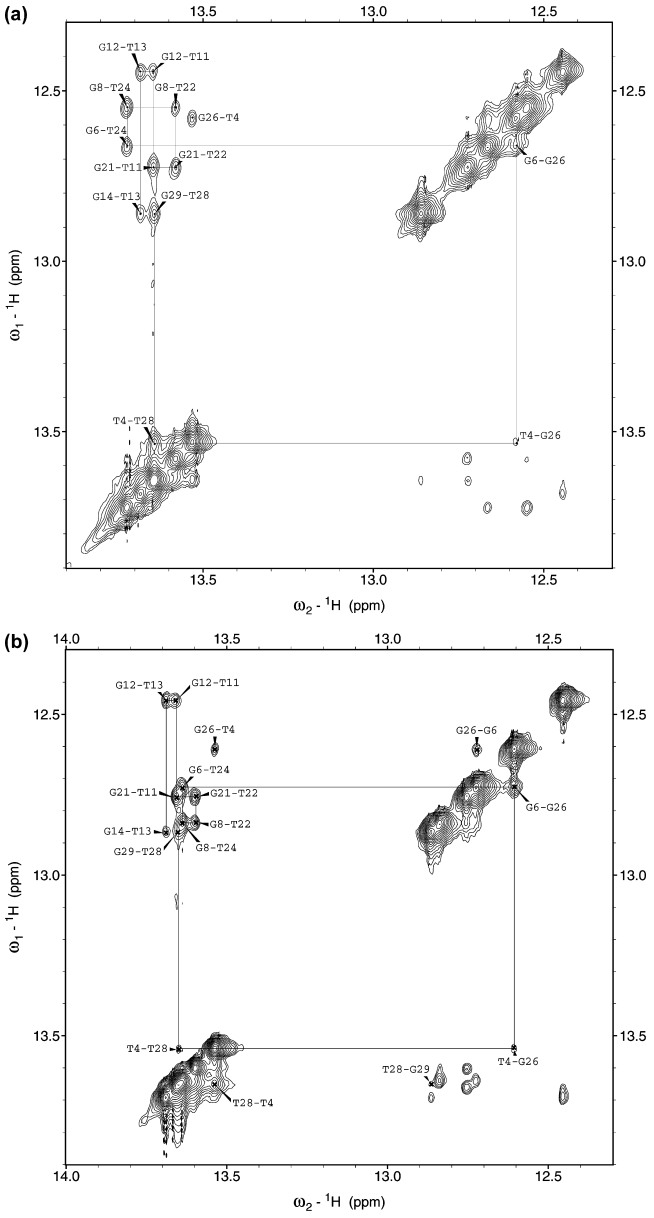

Figure 3. Imino–imino 2D NOESY spectra. These spectra show through-space coupling between guanine N1 and thymine N3 imino protons in neighboring base pairs for (a) parent duplex **1**–**2** and (b) 8oxoG lesion duplex **1oxo**–**2**. Cross-peaks in this region were assigned by tracing them consecutively from one end of the helix (G_{29}) to the other (G_{14}), as shown with solid lines. Thymine imino proton resonances are found between 13.5 and 14 ppm and guanine imino proton resonances between 12.4 and 12.9 ppm, so the peaks farthest from the diagonal correspond to G-T and T-G steps; peaks close to the diagonal correspond to G-G or T-T steps. Note that the terminal guanine imino protons exchange too quickly to be seen on the time scale of this NOESY experiment.

NOESY spectra for the parent and 8oxoG lesion duplex are quite similar in every region in terms of peak shape, intensity, and chemical shift (for example, Figure 5 of the Supporting Information). A careful measurement of chemical shift differences between lesion and parent duplex spectra shows that, not surprisingly, the most marked differences between parent and lesion duplex occur in the base and sugar protons immediately flanking the 8oxoG lesion and in the cytosine Watson–Crick partner (Table 4 of the Supporting Information). To facilitate visualization of the locations and magnitudes of observed changes, we constructed a simple model of parent duplex **1**–**2** using Nucleic Acid Builder and color-coded the chemical shift differences observed in lesion duplex **1oxo**–**2** (Figure 4). The A_7 and A_9 aromatic H8 protons, the C_{23} amino protons, the T_{24} imino proton, and the A_7 and G_8 sugar proton resonances show the largest differences between the lesion duplex and parent duplex; the G_8 H1′ proton disappears altogether. Overall, modest but measurable differences in chemical shift were observed in the 2–3 bp flanking the lesion, particularly on the lesion strand. The chemical shifts of the nucleotides more than 3 bp from the 8oxoG are not perturbed by the presence of the lesion (within the error of measurement, i.e., <0.02 ppm).

Exploring 8oxoG Lesion Base Pair Stability Using the Exchange Rate of the Guanine N1 and Thymine N3 Imino Protons. We chose this 15-mer duplex from a group of duplex sequences on the basis of the generally good dispersion of the imino proton resonances in both parent and 8oxoG lesion duplexes, as measured in phosphate buffer at pH 7.5 and 8 °C. Assignment of the 2D NOESY spectra allowed us to unequivocally identify these peaks in the 1D ^{1}H NMR spectrum (Figure 5). As is generally the case, the thymine N3 imino resonances are found slightly downfield from the guanine N1 imino resonances. The 8oxoG_8 N1 imino peak is shifted downfield compared to that of its parent G_8 by 0.28 ppm, and the T_{24} imino, which flanks 8oxoG_8's cytosine complement, shifts upfield by 0.09 ppm. However, the remainder of the imino proton resonances change very little upon going from parent to lesion duplex. The peaks corresponding to the terminal guanines G_{16} and G_{30} are short and broad due to fraying of the DNA duplex, but the single large peak corresponding to both G_{29} and G_{14} (the penultimate guanines located 1 bp in from the ends of the duplex) is sharp. Notably, the 8oxoG_8 N1 imino proton resonance is not broadened, and its amplitude is equivalent to that of the other guanines, indicating that it is base paired and stacked much like a normal guanine. In contrast, the 8oxoG_8 N7 imino proton resonance is significantly smaller and broader, as expected for an imino proton facing outward into the major groove (Figure 5B, inset).

With the imino proton assignments in hand, we set out to measure the exchange rate of these protons with water as a handle for exploring the stability and dynamics of the 8oxoG-C base pair and its neighbors in double-helical DNA as described by Guéron,[36,48] Russu,[49,50] Stivers,[22,23] and their respective co-workers. Magnetization transfer from water protons is used to measure the exchange rate of DNA imino protons because this rate is too fast to measure by direct titration of deuterium oxide in real time. Plots of the amplitude of each imino peak as a function of mixing time show that protons on the internal bases (i.e., G_6, G_{12}, or G_{21}) exchange less with the solvent than those near the end (the peak corresponding to the penultimate bases G_{29} and G_{14}, and the terminal peak labeled term, corresponding to either G_{16} or G_{30}) (Figure 6). Interestingly, the curve corresponding to the 8oxoG_8 imino proton is similar to that of the other internal guanine protons. Each curve was fitted to eq 4 to estimate an exchange rate (k_{ex}) for each proton in the duplex. To deconvolute overlapping peaks, the values of k_{ex} were further refined by a multiparameter fit of the whole set of spectra at all time points as described in Materials and Methods (Tables 5 and 6 and Figure 6 of the Supporting Information).

Unfortunately, these imino proton exchange rates do not directly reveal the rate or equilibrium constant of base pair

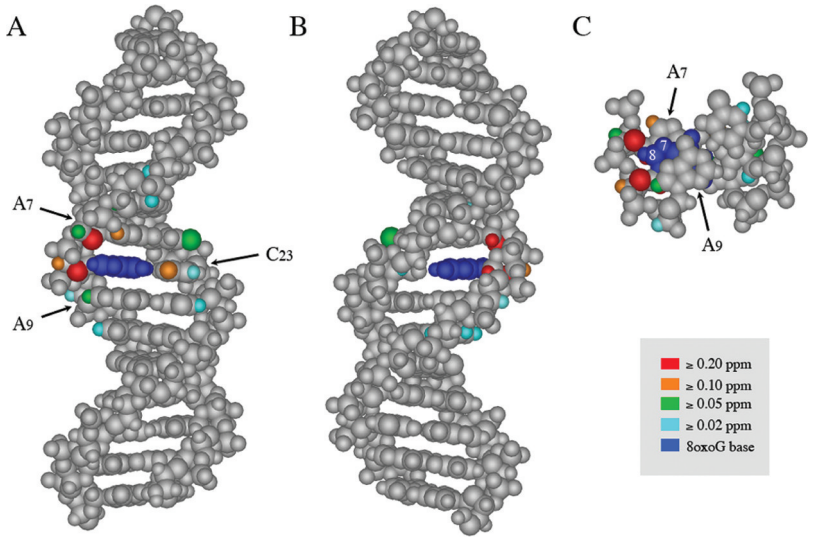

Figure 4. Chemical shift differences between parent and 8oxoG duplex NOESY spectra. Model of duplex **1**−**2** shown (A) from the major groove, (B) from the minor groove, and (C) along the helical axis. Each model is color-coded as indicated in the legend to indicate the magnitude of differences in chemical shift between protons on the parent and lesion duplexes. The base of G_8 is colored royal blue for the sake of clarity; the chemical shift of its imino proton changes significantly because of major electronic differences between guanine and 8oxoG. The default gray color indicates that (1) the chemical shift of the proton did not change (i.e., the protons on the terminal 4 bp at either end of the duplex), (2) the proton chemical shift was not assigned (i.e., the H4′ and H5′ protons), or (3) the atom is not a hydrogen and/or does not have a hydrogen attached to it that could be assessed by this method (i.e., backbone phosphates, portions of the aromatic bases). The values of all of the chemical shifts included in this figure are listed in Table 4 of the Supporting Information. Where protons could be measured spectroscopically but are not shown explicitly in this diagram, the carbon or nitrogen to which they are attached has been shaded instead. In panels A and B, the C_1-G_{30} base pair is shown at the top of the duplex. In panel C, only nucleotides A_7-G_8-A_9 and their complements are shown; the guanine N7 and C8 positions are labeled with white numbers.

opening, because the base pair may open and close many times without exchanging a proton with the solution. Thus, the values of k_{ex} determined in sodium phosphate buffer dramatically underestimate the rate of base pair opening. To increase the rate of imino proton exchange with solvent, we titrated in a glycine base catalyst and determined the exchange rate of each imino proton at each concentration point as described in the previous paragraphs. The exchange rates determined for each imino proton on the parent and 8oxoG lesion duplex are shown in histogram form for three concentrations across the range tested: 5, 100, and 1000 mM glycine (Figure 7). Note that T_{24}, T_{28}, and T_{11} are not included in the histogram because these peaks overlap substantially in the 8oxoG lesion duplex 1D spectrum. The peaks for penultimate bases G_{29} and G_{14} also overlap completely, but because of their similar location in the sequence (i.e., with a terminal GC base pair to their 3′ side) and similar flanking sequence (a thymine to the 5′ side), we assumed for the purposes of calculation that they behaved identically.

At a total glycine concentration of 5 mM (12.5 μM active base), the lowest concentration of base catalyst, the terminal proton (G_{16} or G_{30}) and the 8oxoG outward-facing N7 have the largest exchange rates on the order of ∼100 s^{-1} (Figure 7A,B). The k_{ex} of the other imino protons is significantly smaller, on the order of 2 s^{-1}, and is similar for the parent and lesion duplex (blue and red, respectively). Notably, the rate of exchange of the 8oxoG_8 base-pairing N1 proton is only slightly faster than that of the corresponding proton in the parent duplex (red arrow). By a total glycine concentration of 100 mM (250 μM base catalyst), the peaks corresponding to the terminal base imino proton and 8oxoG_8 N7 proton have become too small and broad to measure, consistent with fast exchange of protons not involved in stable, long-lived hydrogen bonds. The exchange rate of penultimate residues G_{29} and G_{14} increases to ∼7 s^{-1}, but the k_{ex} of the other imino protons increases only subtly (Figure 7C). By a total glycine concentration of 1000 mM (2.5 mM base catalyst), the exchange rate of penultimate residues G_{29} and G_{14} increases to >20 s^{-1}, but the k_{ex} of the other imino protons still hovers around 3 s^{-1} (Figure 7D). Even at this heightened glycine concentration, the exchange rate of the 8oxoG N1 proton is only slightly higher than that of the parental G_8 proton.

To determine whether the 8oxoG-C base pair is destabilized and open to solvent more than an unmodified guanine, we plotted these exchange rates as a function of glycine catalyst concentration (Figure 8) and fit the resulting lines to eq 8 to obtain the apparent equilibrium constant for base pair opening, αK_{op}. It is clear from eq 8 that the slopes of the lines in Figure 8 are proportional to αK_{op} and k_B (a constant describing the bimolecular collision rate, calculated as described in Materials and Methods), while the intercept is equal to the product of αK_{op} and k_{int}, the rate of intrinsic catalysis by bases in the DNA. Because of their steep slope, G_{29} and G_{14} clearly have a larger equilibrium constant than the other base pairs, and therefore, these base pairs must be open to solvent more than the others, consistent with their location adjacent to the ends of the duplex. The lines for the remaining bases have a shallow slope consistent with apparent equilibrium constants on the order of $\leq 10^{-6}$. Values of αK_{op} and k_{int} determined from fits to these data are listed in Table 2. Most importantly, within the error established here, the equilibrium constant for the opening of the 8oxoG_8 base is not larger than that of its matched guanine G_8 in the parent strand or other similar guanines in either duplex.

To determine directly the rate of base pair opening (k_{op}) of the 8oxoG_8 base and the other DNA bases, we would have to

dx.doi.org/10.1021/bi201007t | *Biochemistry* 2011, 50, 8463−8477

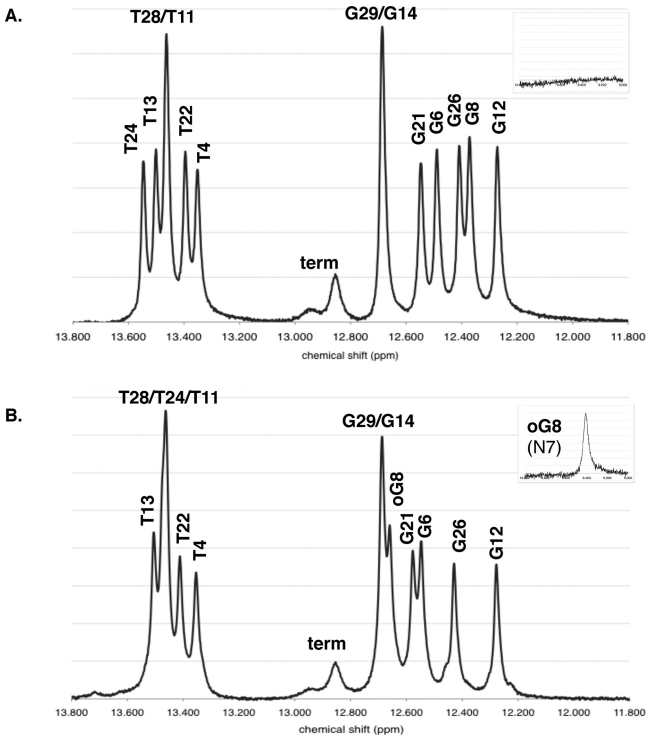

Figure 5. Imino proton region of 1D ^{1}H NMR spectra of (A) parent duplex **1**−**2** and (B) lesion duplex **1oxo**−**2** at 8 °C and pH 7.5. An additional small, broad proton resonance can be seen around 9.4 ppm in the 8oxoG lesion duplex spectrum in the absence of catalyst, corresponding to the N7 imino proton of the 8oxoG lesion itself (inset). Because guanine does not normally have an N7 imino proton, this peak is missing from the parent duplex. "Term" refers to the terminal G_{16} and G_{30} protons with chemical shifts of ∼12.9 ppm.

increase the concentration of glycine base beyond 2.5 mM (1000 mM total glycine). However, it is clear that even below 1000 mM, glycine modifies the structure of the DNA. At 100 mM glycine, the melting temperature behavior of the duplex changes, with the T_m shifting ∼1 °C lower (Figure 9A). This decrease in melting temperature contrasts directly with the behavior for ammonia, another exchange catalyst commonly used in these types of experiments, which significantly stabilizes the DNA at a concentration of 100 mM, increasing the T_m by ∼4 °C. We directly observed this change in DNA structure in the NMR spectra as well. With an increasing glycine concentration, all of the imino peaks move gradually upfield. The guanine peaks generally retain their chemical shifts relative to one another, but the thymine peaks move significantly relative to one another, changing the pattern of overlapping and distinct peaks (Figure 9B). These shifts indicate that some changes in the electronic environment of the bases are occurring with an increasing glycine concentration, and that these changes are not evenly distributed across the duplex. Thus, the values of αK_{op} and k_{int} reported above are based upon data obtained at only ≤600 mM, and no efforts were made to continue the titration beyond 1000 mM glycine.

Direct measurement of the rate of 8oxoG-C base pair opening and closing proved to be impossible with the glycine catalyst at pH 7.5. Glycine is a stronger base than ammonia and therefore in theory a better catalyst; the zwitterionic inactive form might be expected to bind the DNA less strongly than ammonium, and indeed, the duplex melting temperature shows a smaller perturbation at a concentration of 100 mM by glycine than ammonia (Figure 9A). Even so, far too little of the catalyst is active at this pH to efficiently abstract protons from the DNA, and the size and negative charge of the active catalyst form restrict its ability to access the imino protons effectively.

DISCUSSION

The 8-oxoguanine lesion is believed to be formed at the staggering rate of thousands per mammalian cell per day, and if left unrepaired, it can have dire effects upon the cell and the organism.[1,51] Over the past two decades, several groups have explored the structure and thermodynamic stability of 8-oxoguanine and have observed that DNA containing 8oxoG tends to be similar to unmodified DNA.[10,11,15,52] This apparent similarity raises the question of how it can be detected and repaired at all. Here we brought to bear a variety of different types of experiments on the same nonpalindromic 15-mer duplex containing a single centrally located 8oxoG lesion, specifically looking at base pair opening as an unstudied and potentially critical factor in discrimination between lesion and normal guanine.

Structural and Thermodynamic Effects of the 8oxoG Lesion on DNA. Using circular dichroism spectropolarimetry, we confirmed that our 8oxoG duplex is B-form and globally unperturbed by the lesion, as seen previously with 8oxoG in other sequences.[15,52,53] The broad band around 275 nm that is a composite of $\pi \rightarrow \pi^*$ and $n \rightarrow \pi^*$ electronic transitions on the DNA bases changes slightly upon addition of the lesion, in this case its magnitude decreasing slightly but in some cases increasing slightly (Figure 1A).[15,44,52,53] The shape and intensity of this band have been described as reflecting π stacking, indirectly reporting about changes in helical twist and base pair tilt.[54] However, the electron distribution and dipole moment of 8oxoG are quite different from those of unmodified guanine.[7,8] Considering that the molar extinction coefficient for the UV absorption of 8oxoG at 260 nm is less than that of guanine by ∼6300 M^{-1} cm^{-1}, it is not unreasonable to hypothesize that the changes we see in the CD spectrum of the lesion duplex are largely due to localized electronic changes on the lesion base rather than larger structural ones.

This picture of a structurally conserved duplex with electronic differences localized to the lesion site is supported by comparison of NOESY spectra of parent duplex **1**−**2** and lesion duplex **1oxo**−**2** (Figure 3 and Figures 3−5 of the Supporting Information). The imino−imino NOE walk is thoroughly conserved past the lesion base, showing that base pairing is stable at the lesion. The H1′−aromatic base walk and H2′/H2″−aromatic base walk are also thoroughly conserved on the complementary strand, indicative of a B-form helix. As expected, the H8 aromatic proton on the lesion strand is missing at the 8oxoG lesion site, but a thorough search for all possible cross-peaks shows the $8oxoG_8$ H1′ sugar proton to be missing completely from the spectrum also. It seems most likely that the H1′ resonance has shifted from 5.459 ppm in the parent to ∼4.7 ppm in the lesion strand (disappearing under the residual water resonance), reflecting the dramatically different electronic environment it experiences directly 3′ to the 8-oxo group (Figure 4C). The neighboring $8oxoG_8$ H2″ proton resonance moves by more than 0.5 ppm downfield, so by comparison, a 0.67 ppm upfield change in the H1′ chemical shift seems logical in both magnitude and direction. The H1′ proton is more shielded in the lesion duplex than the parent, but the H2″ proton is more deshielded in the lesion duplex. Because of their slightly different positions under the lesion

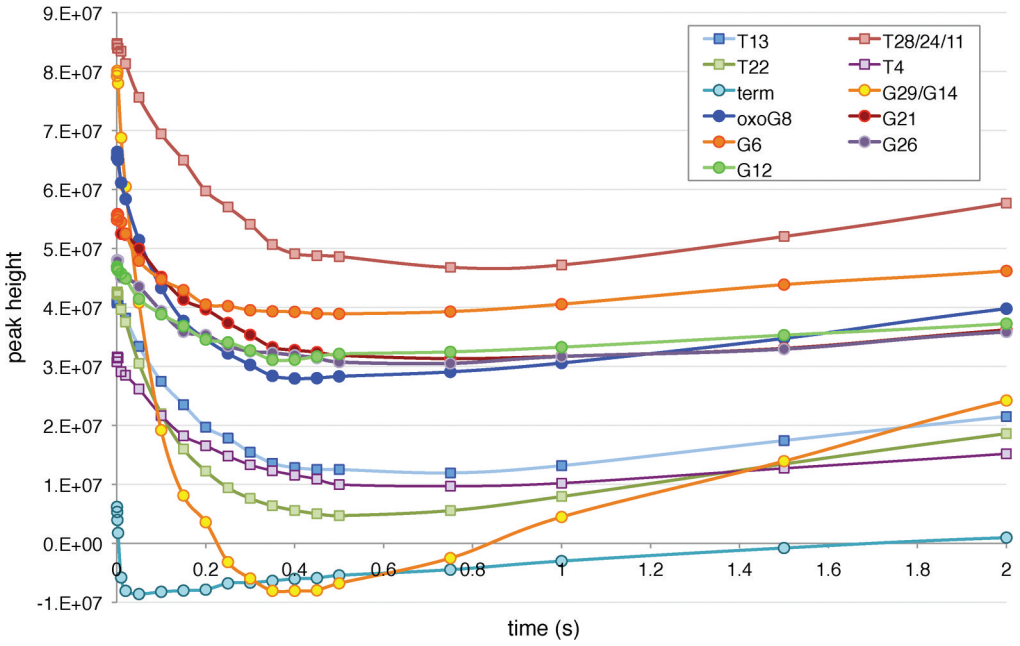

Figure 6. Imino proton intensity as a function of time after selective inversion of water protons. Peak heights evolve as a function of mixing time for lesion duplex **1oxo−2** in the absence of an exchange catalyst. The peak intensities decrease modestly as the imino protons exchange with inverted water protons and then increase as they relax back to their equilibrium value. The curves were fit to eq 4 to determine the exchange rate of the imino proton.

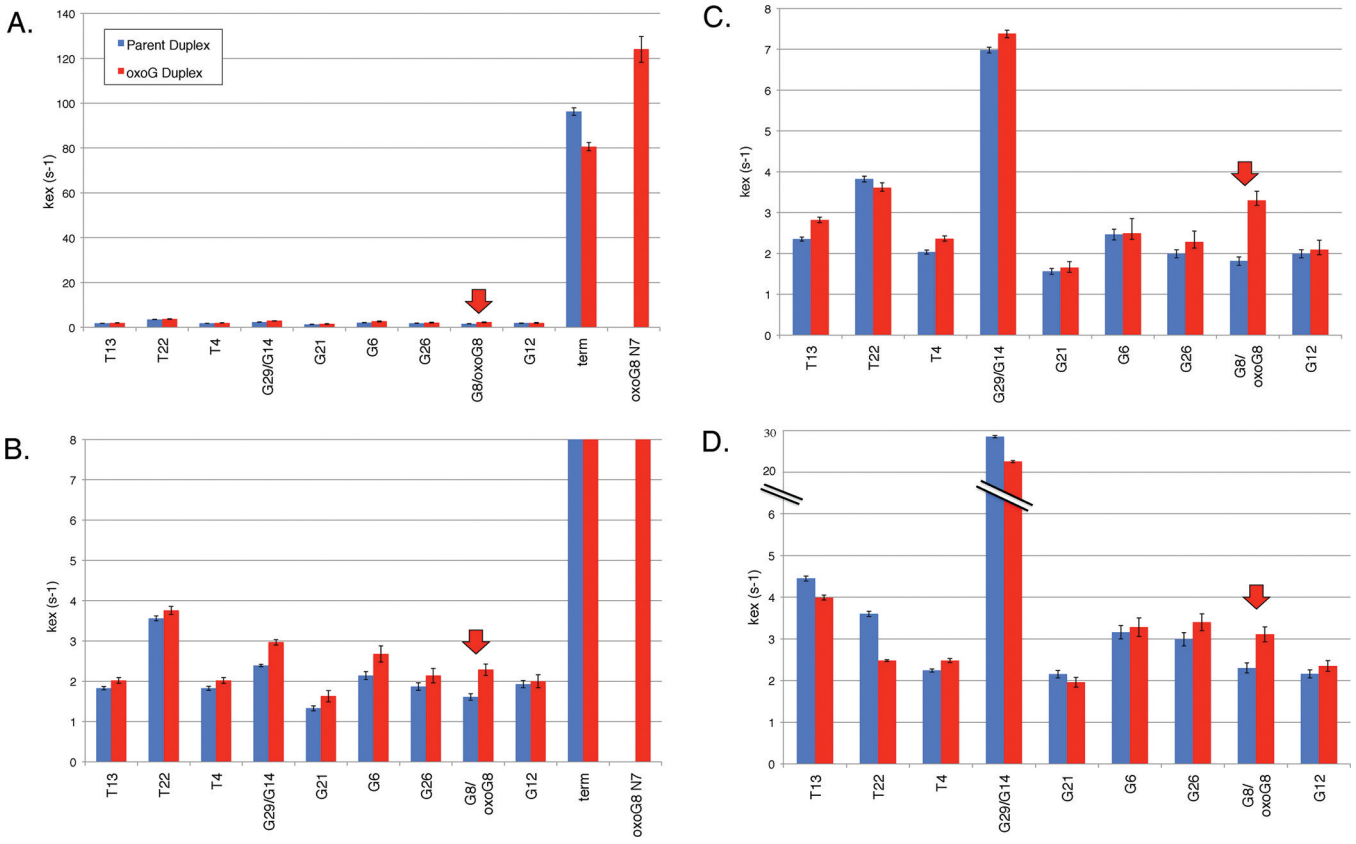

Figure 7. Exchange rate of DNA imino protons at three concentrations of glycine catalyst. In each histogram, the k_{ex} values for base imino protons in the parent (blue) and 8oxoG lesion (red) duplexes are shown in pairs: (A) 5 mM total glycine (12.5 μM active glycine base catalyst) illustrating the exchange rate of one of the terminal peaks and the 8oxoG N7 imino proton, both of which are quite accessible to solution and exchange much more quickly than the internal imino protons, (B) 5 mM total glycine (12.5 μM base) with the y-axis adjusted to illustrate the exchange rates of the internal imino protons, (C) 100 mM total glycine (250 μM base), and (D) 1000 mM total glycine (2.5 mM base).

dx.doi.org/10.1021/bi201007t | *Biochemistry* 2011, 50, 8463–8477

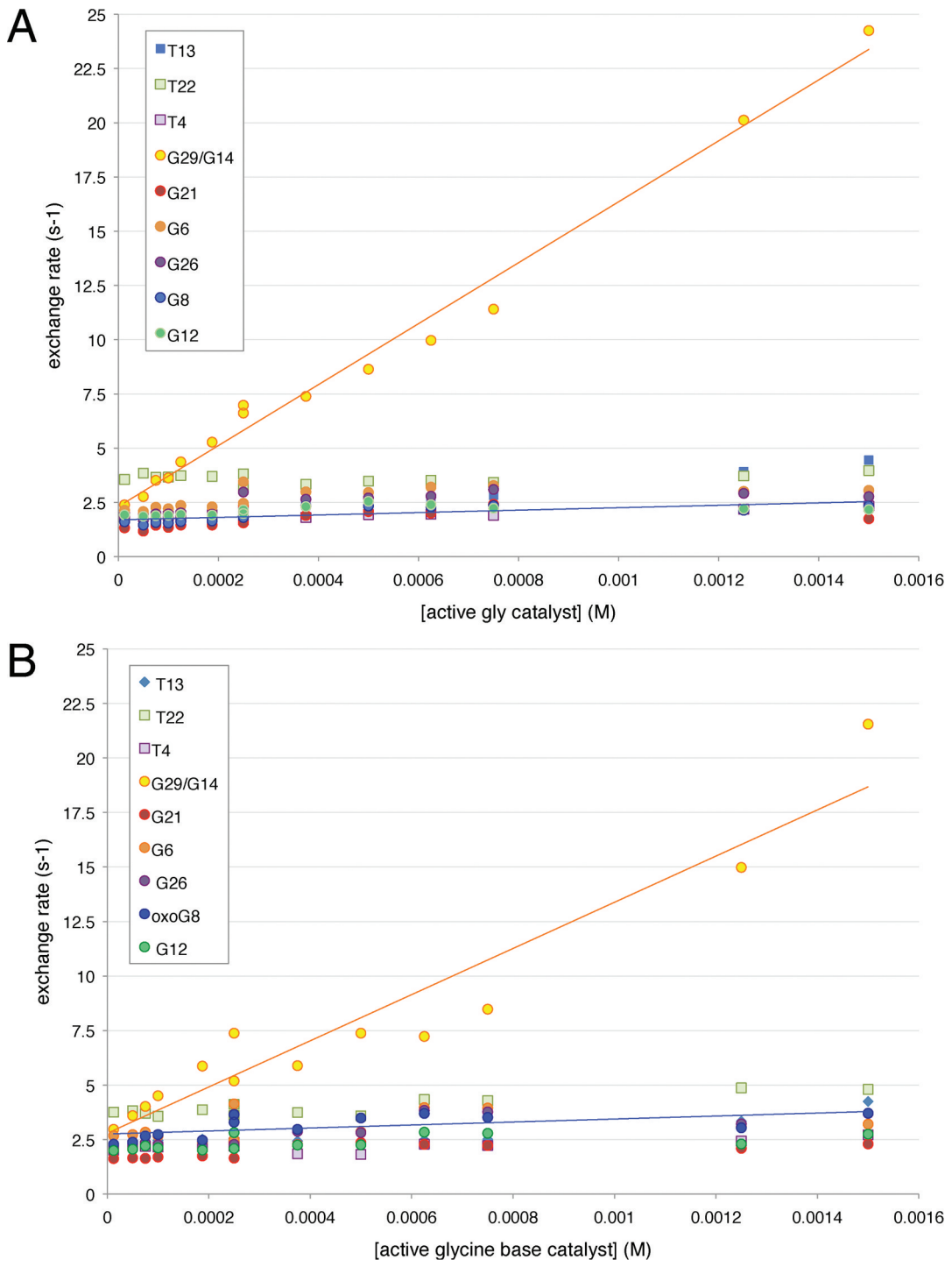

Figure 8. Imino exchange rates in parent and lesion duplexes. The exchange rates of individual protons are shown as a function of glycine catalyst concentration. Data for guanine imino protons are depicted with circles (G_8/8oxoG_8 in blue) and those of thymine imino protons with squares. (A) Exchange rate of imino protons in parent duplex **1**−**2** between 12.5 μM and 2.5 mM base catalyst. Best-fit lines to eq 8 of the G_{29}/G_{14} exchange rates and G_8 exchange rates are shown. (B) Exchange rate of imino protons in lesion duplex **1oxo**−**2** between 12.5 μM and 2.5 mM base catalyst. Best-fit lines to eq 8 of the G_{29}/G_{14} exchange rates and 8oxoG_8 exchange rates are shown.

base, each proton experiences a unique, and clearly opposite, change in its electronic environment due to the 8oxoG base dipole.[10] However, without either the aromatic or the H1′ resonance, it is difficult to establish whether the 8oxoG_8 sugar pucker is different from that of the parent because of crowding from the extra carbonyl oxygen at the 8 position. Early structural data are inconclusive on this point, but recent crystallographic evidence points to a C2′-*endo* configuration on the 8oxoG nucleotide's sugar in a different duplex sequence.[12]

A quantitative comparison of proton chemical shifts throughout the duplex reveals that changes are highly localized to the bases and sugars closest to the lesion site, consistent with the only other published NOESY spectrum of DNA containing 8oxoG-C base pairs (Figure 4).[10] Because our oligonucleotide duplex is 15 bp long with seven normal base pairs on either side

dx.doi.org/10.1021/bi201007t | *Biochemistry* 2011, 50, 8463–8477

Table 2. Base Pair Exchange and Opening Parameters[a]

	$\alpha K_{op} \times 10^6$		k_{int} ($\times 10^{-6}$ M^{-1} s^{-1})	
	duplex **1**−**2**	duplex **1oxo**−**2**	duplex **1**−**2**	duplex **1oxo**−**2**
G_{29}/G_{14}	35 ± 2	22 ± 3	0.068 ± 0.005	0.15 ± 0.03
G_8 or $oxoG_8$	1.8 ± 0.4	1.6 ± 0.6	0.87 ± 0.2	1.7 ± 0.6
G_{21}	1.7 ± 0.5	1.1 ± 0.4	0.81 ± 0.2	1.6 ± 0.6
G_6	2.2 ± 0.5	1.3 ± 0.7	1.0 ± 0.2	2.1 ± 1.1
G_{26}	2.4 ± 0.5	2.8 ± 0.7	0.81 ± 0.2	0.81 ± 0.2
G_{12}	0.77 ± 0.3	0.97 ± 0.4	2.4 ± 0.9	2.1 ± 0.8
T_{13}	4.8 ± 0.3	3.1 ± 0.7	0.38 ± 0.02	0.70 ± 0.2
T_4	0.84 ± 0.2	1.0 ± 0.4	2.1 ± 0.5	1.9 ± 0.8

[a] αK_{op} is the the apparent equilibrium constant for base pair opening; k_{int} is the intrinsic rate of imino proton exchange.

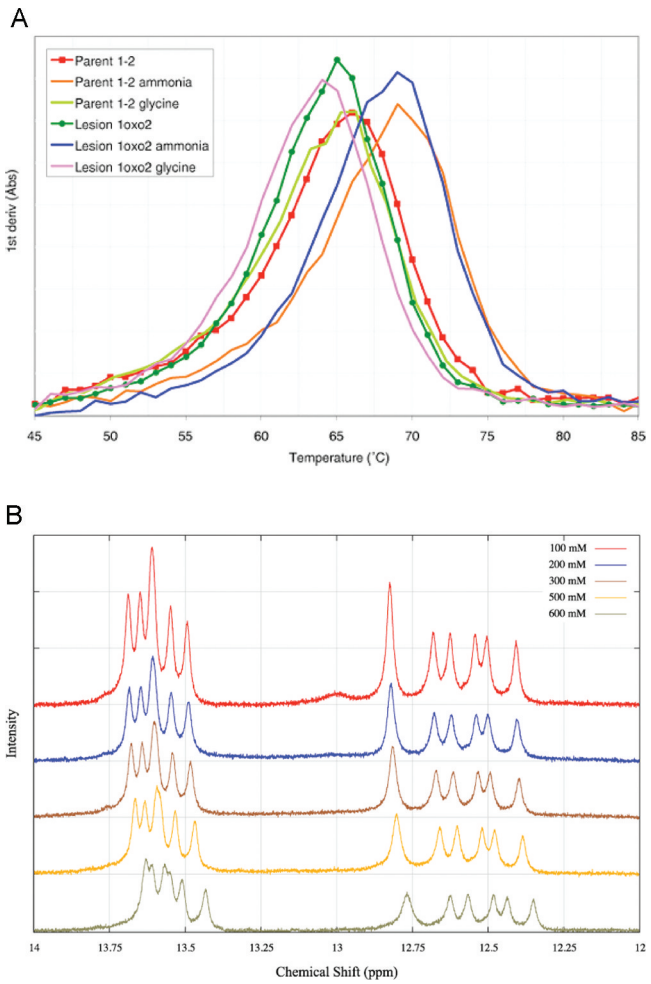

Figure 9. Effect of glycine titrant on DNA stability and structure. (A) First derivatives of UV melting curves for parent and lesion duplexes at a duplex concentration of 5 μM with either no added catalyst, 100 mM glycine, or 100 mM ammonia. (B) Glycine-dependent changes in the imino proton chemical shift in parent duplex **1**−**2**.

of the lesion, we can uniquely demonstrate that the effects of the lesion weaken greatly with distance. Indeed, no difference in chemical shift is seen for protons on nucleotides more than 3 bp from the lesion. Protons on the complementary strand are significantly less affected by the lesion, with the exception of the C_{23} N4 amino proton and the T_{24} imino proton. Because the C_{23} N4 amino proton is directly hydrogen-bonded to the 8oxoG lesion base, it should be particularly sensitive to electronic changes to that guanine. Similarly, the T_{24} imino proton is stacked immediately below the 8oxoG base. In contrast, the C_{23} C5 and C6 aromatic protons, which point outward toward the major groove and away from the 8oxoG lesion base, display much smaller changes in chemical shift, supporting the idea that 8oxoG's primary effect on duplex DNA structure could be electronic rather than steric. Such electronic effects may serve as a distinctive repair signal in the absence of large structural distortions.[55,56]

Having seen that the structure of this nonpalindromic 15-mer duplex containing an 8oxoG-C base pair is essentially the same as its control duplex in terms of overall shape and conformation, we also probed the thermodynamic stability of the duplexes. A van't Hoff analysis of UV melting revealed that in this relatively long duplex, the 8oxoG lesion has almost no effect on the overall double strand−single strand equilibrium (Figure 1B,C), consistent with 8oxoG's effects measured by other groups using shorter duplexes and/or different flanking sequences.[15,52,53] Similarly, the mismatch-sensitive photocleavage agent $Rh(bpy)_2(chrysi)^{3+}$ was unable to detect the presence of 8oxoG in this 15-mer duplex. The latter result is particularly interesting because $Rh(bpy)_2(chrysi)^{3+}$ has been shown to detect some mismatch sites much more effectively than others, reflecting primarily local thermodynamic stability and also steric or kinetic factors. This differential cleavage allows us to roughly rank the plasticity of the 8oxoG-C site within a range of noncanonical sites.[46,47] The more stable mismatches that can stack well and form some hydrogen bonds, such as a G-A mismatch, are poorly bound and cleaved by $Rh(bpy)_2(chrysi)^{3+}$, whereas open, unstable mismatches such as CC mismatches are detected robustly. Within this context, the 8oxoG-C pair seems to be less open and accessible than a pyrimidine-pyrimidine mismatch. Furthermore, the fact that the 8oxoG site was not bound and cleaved efficiently, even when we mispaired it with adenine, points to the fact that the double helix is locally stable at the site of the 8oxoG and not just globally stable as revealed by the van't Hoff analysis.

Effect of the 8oxoG Lesion on Base Pair Opening. To discover whether the 8oxoG lesion has a kinetic or dynamic effect on the DNA helix, we set out to determine the rate of base pair opening for all of the bases in the lesion and control duplex. Fortunately, unlike some base lesions, the 8oxoG lesion retains the imino proton of its unmodified precursor, giving us the handle to examine base pair opening. Even between 5 and 100 mM glycine, it is clear that the rate of exchange of the 8oxoG imino proton is similar to those of most of the internal guanines but distinctly different from those of the terminal bases, the penultimate bases G_{29} and G_{14}, and the 8oxoG N7 imino proton (Figure 7). The 8oxoG N7 proton provides a fascinating internal control given that it is located on the same lesion base only a few angstroms from N1. The $8oxoG_8$ N7 imino proton exchanges much more quickly than the N1 imino proton even though it is much slower to tautomerize and its pK_a is calculated to be almost 4 pH units higher.[7,9] The fact that the N7 proton exchanges so rapidly with the solution confirms that it faces outward into the major groove rather than toward the complementary cytosine, in direct contrast with N1. The terminal bases also exchange very quickly because they need not strictly open to the solution to exchange their imino proton; solvent molecules can approach the face of the bases directly even when the bases are stacked and base-paired, and as a result, they can abstract protons with facility. The penultimate

dx.doi.org/10.1021/bi201007t | Biochemistry 2011, 50, 8463−8477

bases G_{29} and G_{14} provide an interesting third comparison. As guanines they are reasonable controls for the 8oxoG sterically and electronically, and they do lack the direct steric access issues of the terminal bases. However, even at 8 °C, the ends of the DNA duplex fray, and the base pairing face becomes accessible to the solution. These penultimate base pairs open slowly and infrequently enough to have sharp NMR resonances even at the highest glycine concentrations, but they are clearly more mobile and/or accessible to solution than the internal bases. The 8oxoG exchange rates are distinct from all of these, being similar to but slightly larger than that of the corresponding guanine G_8 in the parent duplex (Figure 7 and Figure 7 of the Supporting Information). Though this slight difference might appear to indicate a difference in opening rate or thermodynamics, it must be noted that the 8oxoG imino proton has a pK_a around 0.7 pH unit lower than that of normal guanine, meaning that it is more acidic and therefore easier to deprotonate.[7] When the difference in pK_a is taken into account (the k_B term in eq 8), the apparent equilibrium constant for base pair opening of the 8oxoG base is essentially the same as that of the corresponding parental base G_8, and the other internal guanine bases (Table 2). The fact that the intrinsic rate of exchange of a proton from the 8oxoG base is slightly larger than the rate of exchange from the parental control base is probably due to the same pK_a effect.

At the glycine concentrations measured, abstraction of most of the imino protons is quite inefficient and the slopes of the lines in Figure 8 are shallow; as a result, the errors in our estimates of guanine αK_{op} values are on the order of 20−30%. Thus, it is quite possible that the apparent equilibrium constant for opening of the 8oxoG-C is slightly larger than that of a control GC pair. Nonetheless, we can exclude the possibility of 8oxoG's αK_{op} being much larger than that of G_8 on the basis of the upper bound provided by the penultimate bases G_{29} and G_{14}, which have equilibrium constants that are 10 times larger but also exchange at a rate that is clearly distinct from that of 8oxoG. Note that apparent equilibrium constants on the order of 10^{-6} agree with those measured by this method in other short DNA duplexes.[22,36] Depending on the value of α, this equilibrium constant is equivalent to a free energy cost for breaking a base pair between 6 and 7 kcal/mol, consistent with calculated energy costs for breaking G-C and 8oxoG-C base pairs.[24,41,57]

Because the apparent equilibrium constant αK_{op} is the same for 8oxoG as for the other guanine bases, we can say that the overall fraction of time that the 8oxoG-C base pair spends open to solution is the same as the amount of time that a G-C base pair spends open (i.e., one-millionth). However, we could not directly determine the rates of base pair opening (k_{op}) and closing (k_{cl}) because imino exchange was too weakly catalyzed over this range of glycine concentrations. As a result, we cannot exclude the possibility that the rate of 8oxoG-C base pair opening is faster than the rate of G-C base pair opening. If that were the case, any increases in the rate of opening would have to be matched by equivalent increases in the rate of base pair closing because αK_{op} is equal to the ratio of the opening and closing rates (eq 6). Conversely, an open 8oxoG-C base pair might conceivably close more slowly than a G-C base pair, but then it would also have to open more slowly. Either might facilitate detection and repair, the former by decreasing the activation energy of base pair opening and the latter by prolonging the lifetime of the extrahelical state (Figure 10).

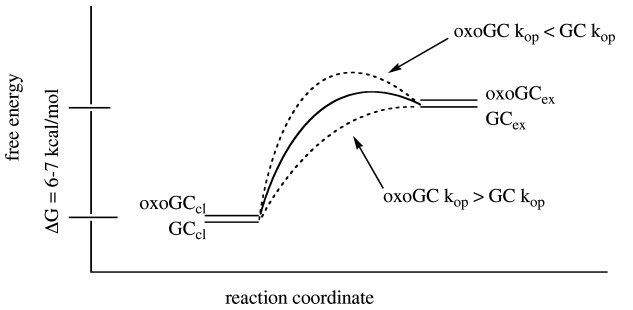

Figure 10. Reaction coordinate diagram illustrating exchange from the G-C and 8oxoG-C base pairs. The free energy difference between the closed state (GC_{cl} and $oxoGC_{cl}$) and the "open" state available for imino proton exchange (GC_{ex} and $oxoGC_{ex}$) is 6−7 kcal/mol, due to the cost of breaking three hydrogen bonds and unstacking one or both bases from the hydrophobic core of the helix. The two base pairs are shown with similar stabilities in both closed and exchangeable states because every method used in this study has found the oxoG-C base pair to be almost indistinguishable from the G-C base pair. Critically, many other open forms are likely to exist along the reaction coordinate pathway with energies similar to or higher than the energies of GC_{ex} and $oxoGC_{ex}$, but these are not shown because they are not directly probed by this experiment. Dashed lines illustrate the effect of increasing or decreasing k_{op} on the activation energy of base pair opening; the latter would extend the lifetime of the open state, and the former would decrease the activation energy of opening.

It is important to remember that this imino proton exchange model assumes a two-state, open-or-closed model of base pair opening, when in fact that is unlikely to be the case.[36] Molecular dynamics simulations suggest that the purine base, the pyrimidine base, or both might rotate out of the helix to open to solvent, and opening may occur through either the major or minor grooves depending on the steric and energetic limitations.[57] "Opening" itself is a slightly murky term, because the bases do not have to swing out by 180° or even 90° to make possible hydrogen exchange between solvent protons and base imino protons.[58,59] Nevertheless, breaking the hydrogen bonds and unstacking at least one base from the hydrophobic core of the helix, i.e., the energetic barrier measured by proton exchange measurements, is not only the initial step but also likely the largest energetic contributor to any opening process. The free energy associated with this critical step appears to be the same for the 8oxoG-C base pair as for a GC base pair.

DNA can be considered a dynamic molecule over many time scales, ranging from short-range vibrational and electronic fluctuations occurring at subpicosecond time scales, to bending and twisting motions occurring on the picosecond to nanosecond time scales, to base pair opening on the microsecond to millisecond time scales, to a variety of large-scale, activated, or cooperative processes occurring at longer times.[48,60,61] Given the critical role of base pair flipping in glycosylase mechanisms, we chose to focus on changes in spontaneous base pair opening dynamics around the 8oxoG lesion. However, the bending, curvature, or dynamic movement of 8oxoG-containing DNA on other time scales or other size scales may yet prove to be more distinctive than the base pair opening dynamics.[16,62]

Enzymatic detection of 8oxoG-C base pairs may exploit other subtle differences between lesion and normal base pairs. Subtle changes to water molecule and cation binding around an 8oxoG-C base pair, with corresponding small changes to sugar−phosphate backbone angles, have been predicted

computationally[18] and demonstrated experimentally using calorimetric methods and γ-ray footprinting.[52,63]

Biological Implications for 8-Oxoguanine Repair. Extensive work on the mechanisms of DNA base excision repair glycosylases has demonstrated that they bind the DNA nonspecifically and quickly scan the genome for lesions by sliding along the DNA for short periods interspersed with hopping.[64] When they find a base lesion, they bind it extrahelically and cleave it at the glycosidic bond.[65] Though the chemistry of the cleavage mechanisms is well understood, the initial enzyme–lesion encounter and recognition events remain an active area of research.[20,66] The evidence presented here that the equilibrium constant for 8oxoG-C base pair opening is the same as that of a normal G-C base pair provides a critical piece of information about the parameters for recognition and extrusion of this lesion. Because 8-oxoguanine remains securely buried in the helix the vast majority of the time, it seems likely that repair enzymes may have to exploit yet-unmeasured differences in opening and closing rates, sense electronic differences between the oxidized and normal base, detect new bending modes or changes to water molecule binding, or actively perturb the DNA to detect the lesion.

■ CONCLUSIONS

Here we have shown that a 15-mer DNA duplex containing an 8-oxoG-C base pair is both globally and locally almost indistinguishable from a control normal duplex. Not only is the lesion duplex B-form and similar in overall thermodynamic stability to the control duplex as shown by CD and van't Hoff analysis, but the immediate vicinity of the lesion is also well-conserved. 2D NOESY spectra reveal that differences between the duplexes are localized to the lesion, with the flanking bases beyond the immediate two base neighbors and most of the complementary strand being completely unaffected by the lesion. The base mismatch agent $Rh(bpy)_2chrysi^{3+}$ shows no clear preference for binding the lesion site over other Watson–Crick sites. Most notably, NMR imino exchange measurements indicate that the intrahelical stability of the 8-oxoguanine-cytosine base pair is the same as that of normal GC base pairs. When taken together, this group of structural and thermodynamic measurements performed side by side on the same nonpalindromic 15-mer duplex confirm that the 8oxoG lesion is indeed well-hidden in a B-form DNA duplex, leaving open continued speculation about how this common promutagenic lesion is detected and repaired.

■ ASSOCIATED CONTENT

Supporting Information

Structures of normal and lesion base pairs, tables of mixing times, melting temperature curves, annotated NOESY spectra, tables of chemical shift assignments, representative Matlab fits, and comparisons of exchange rates between normal and lesion duplexes. This material is available free of charge via the Internet at http://pubs.acs.org.

■ AUTHOR INFORMATION

Corresponding Author

*Department of Chemistry, 50 College St., Mount Holyoke College, South Hadley, MA 01075. Telephone: (413) 538-2449. Fax: (413) 538-2327. E-mail: menunez@mtholyoke.edu.

Funding

This work was supported by the Camille and Henry Dreyfus Foundation, the Clare Boothe Luce Foundation, the Radcliffe Institute for Advanced Study at Harvard University, and the National Institute of General Medical Sciences (1R15GM083250).

■ ACKNOWLEDGMENTS

M.E.N. extends her deepest thanks to Professor Gregory Verdine and his laboratory group for generously providing space for and encouragement of this project. We also thank Professor Gerhard Wagner at Harvard Medical School for use of the 750 MHz NMR to obtain NOESY spectra, Dr. Jean-Christophe Hus for sharing with us his Python scripts for NMR spectral processing in NMR Pipe, Ms. Elisa Frankel for her expertise with DNA melting experiments, Ms. Sara Barnes for gel electrophoresis support, Dr. Mandy Blackburn in the Gierasch lab at the University of Massachusetts for help with CD, and Dr. Jacqueline Barton for the gift of $Rh(bpy)_2chrysi^{3+}$.

■ ABBREVIATIONS

8oxoG, 8-oxo-7,8-dihydro-2′-deoxyguanosine or 8-oxoguanine; NMR, nuclear magnetic resonance spectroscopy; NOESY, nuclear Overhauser effect spectroscopy; BER, base excision repair; PAGE, polyacrylamide gel electrophoresis; CD, circular dichroism spectropolarimetry; HPLC, high-performance liquid chromatography; $Rh(bpy)_2(chrysi)^{3+}$, bis(2,2′-bipyridine)(5,6-chrysenequinone diimine)rhodium(III); k_{ex}, rate of imino proton exchange; k_{op}, rate of base pair opening; αK_{op}, apparent equilibrium constant for base pair opening.

■ REFERENCES

(1) Friedberg, E. C., Walker, G. C., Siede, W., Wood, R. D., Schultz, R. A., and Ellenberger, T. (2006) *DNA Repair and Mutagenesis*, 2nd ed., ASM Press, Washington, DC.

(2) Dedon, P. C. (2011) Oxidation and deamination of DNA by endogenous sources. *Curr. Cancer Res.: Chem. Carcinog.*, 209–225.

(3) Burrows, C. J., and Muller, J. G. (1998) Oxidative nucleobase modifications leading to strand scission. *Chem. Rev. 98*, 1109–1151.

(4) Steenken, S., and Jovanovic, S. (1997) How easily oxidizable is DNA? One-electron reduction potentials of adenosine and guanosine radicals in aqueous solution. *J. Am. Chem. Soc. 119*, 617–618.

(5) Shibutani, S., Takeshita, M., and Grollman, A. P. (1991) Insertion of specfic bases during DNA synthesis past the oxidation-damaged base 8-oxodG. *Nature 349*, 431–434.

(6) Hsu, G. W., Ober, M., Carell, T., and Beese, L. S. (2004) Error-prone replication of oxidatively damaged DNA by a high-fidelity DNA polymerase. *Nature 431*, 217–221.

(7) Jang, Y. H., Goddard, W. A. III, Noyes, K. T., Sowers, L., Hwang, S., and Chung, D. S. (2002) First principles calculations of the tautomers and pK_a values of 8-oxoguanine: Implications for mutagenicity and repair. *Chem. Res. Toxicol. 15*, 1023–1035.

(8) Banerjee, A., Yang, W., Karplus, M., and Verdine, G. L. (2005) Structure of a repair enzyme interrogating undamaged DNA elucidates recognition of damaged DNA. *Nature 434*, 612–618.

(9) Cho, B. P., Kadlubar, F. F., Culp, S., and Evans, F. (1990) ^{15}N nuclear magnetic resonance studies on the tautomerism of 8-hydroxy-2′-deoxyguanosine, 8-hydroxyguanine, and other C8-subsituted guanine nucleosides. *Chem. Res. Toxicol. 3*, 445–452.

(10) Oda, Y., Uesugi, S., Ikehara, M., Nishimura, S., Kawase, Y., Ishikawa, H., Inoue, H., and Ohtsuka, E. (1991) NMR studies of a DNA containing 8-hydroxydeoxyguanosine. *Nucleic Acids Res. 19*, 1407–1412.

(11) Lipscomb, L. A., Peek, M. E., Morningstar, M. L., Verghis, S. M., Miller, E. M., Rich, A., Essigmann, J., and Williams, L. D. (1995) X-ray

structure of a DNA decamer containing 7,8-dihydro-8-oxoguanine. *Proc. Natl. Acad. Sci. U.S.A. 92*, 719−723.
(12) Bowman, B. R., Lee, S., Wang, S., and Verdine, G. L. (2008) Structure of the *E. coli* DNA glycosylase AlkA bound to the ends of duplex DNA: A system for the structure determination of lesion-containing DNA. *Structure 16*, 1166−1174.
(13) McAuley-Hecht, K., Leonard, G. A., Gibson, N. J., Thomson, J. B., Watson, W. P., Hunter, W. N., and Brown, T. (1994) Crystal structure of a DNA duplex containing 8-hydroxydeoxyguanine-adenine base pairs. *Biochemistry 33*, 10266−10270.
(14) Kouchakdjian, M., Bodepudi, V., Shibutani, S., Eisenberg, M., Johnson, F., Grollman, A. P., and Patel, D. J. (1991) NMR structural studies of the ionizing radiation adduct 7-hydro-8-oxodeoxyguanosine (8-oxo-7H-dG) opposite deoxyadenosine in a DNA duplex. 8-Oxo-7H-dG (*syn*)*dA (*anti*) alignment at lesion site. *Biochemistry 30*, 1403−1412.
(15) Plum, G. E., Grollman, A. P., Johnson, F., and Breslauer, K. J. (1995) Influence of the oxidatively damaged adduct 8-oxodeoxyguanosine on the conformation, energetics, and thermodynamic stability of a DNA duplex. *Biochemistry 34*, 16148−16160.
(16) Miller, J. H., Fan-Chiang, C.-C., Straatsma, T. P., and Kennedy, M. A. (2003) 8-Oxoguanine enhances bending of DNA that favors binding to glycosylases. *J. Am. Chem. Soc. 125*, 6331−6336.
(17) Ishida, H. (2002) Molecular dynamics simulation of 7,8-dihydro-8-oxoguanine DNA. *J. Biomol. Struct. Dyn. 19*, 839−851.
(18) Naômé, A., Schyman, P., Laaksonen, A., and Vercauteren, D. P. (2010) Molecular dynamics simulation of 8-oxoguanine containing DNA fragments reveals altered hydration and ion binding patterns. *J. Phys. Chem. B 114*, 4789−4801.
(19) Cheng, X., Kelso, C., Hornak, V., de los Santos, C., Grollman, A. P., and Simmerling, C. (2005) Dynamic behavior of DNA base pairs containing 8-oxoguanine. *J. Am. Chem. Soc. 127*, 13906−13918.
(20) David, S. S., O'Shea, V. L., and Kundu, S. (2007) Base-excision repair of oxidative DNA damage. *Nature 447*, 941−950.
(21) Verdine, G. L., and Bruner, S. D. (1997) How do DNA repair proteins locate damaged bases in the genome? *Chem. Biol. 4*, 329−334.
(22) Cao, C., Jiang, Y., Stivers, J., and Song, F. (2004) Dynamic opening of DNA during the enzymatic search for a damaged base. *Nat. Struct. Mol. Biol. 11*, 1230−1236.
(23) Parker, J., Bianchet, M., Krosky, D., Friedman, J. I., Amzel, L., and Stivers, J. (2007) Enzymatic capture of an extrahelical thymine in the search for uracil in DNA. *Nature 449*, 433−437.
(24) Qi, Y., Spong, M. C., Nam, K., Banerjee, A., Jiralerspong, S., Karplus, M., and Verdine, G. L. (2009) Encounter and extrusion of an intrahelical lesion by a DNA repair enzyme. *Nature 462*, 762−766.
(25) Ivanov, V., and Krylov, D. (1992) A-DNA in solution as studied by diverse approaches. *Methods Enzymol. 211*, 111−127.
(26) Sambrook, J., and Russell, D. W. (2001) *Molecular cloning: A laboratory manual*, 3rd ed., Cold Spring Harbor Laboratory Press, Plainview, NY.
(27) Liu, M., Mao, X., He, C., Huang, H., Nicholson, J. K., and Lindon, J. C. (1998) Improved WATERGATE Pulse Sequences for Solvent Suppression in NMR. *J. Magn. Reson. 132*, 125−129.
(28) Jeener, J., Meier, B. H., Bachmann, P., and Ernst, R. R. (1979) Investigation of exchange processes by two-dimensional NMR spectroscopy. *J. Chem. Phys. 71*, 4546−4653.
(29) Macura, S., and Ernst, R. R. (1980) Elucidation of cross relaxation in liquids by two-dimensional NMR spectroscopy. *Mol. Phys. 41*, 95−117.
(30) Delaglio, F., Grzesiek, S., Vuister, G. W., Zhu, G., Pfeifer, J., and Bax, A. (1995) NMRPipe: A multidimensional spectral processing system based on UNIX pipes. *J. Biomol. NMR 6*, 277−293.
(31) Goddard, T. D., and Kneller, D. G. (2010) *Sparky 3*, University of California, San Francisco.
(32) Wemmer, D. (2000) Structure and Dynamics by NMR. In *Nucleic Acids: Structures, Properties, and Functions* (Bloomfield, V., Crothers, D. M., and Tinoco, I., Eds.) University Science Books, Sausalito, CA.
(33) Hare, D. R., Wemmer, D., Chou, S.-H., and Drobny, G. (1983) Assignment of the non-exchangeable proton resonances of d-(CGCGAATTCGCG) using two-dimensional nuclear magnetic resonance methods. *J. Mol. Biol. 171*, 319−336.
(34) Scheek, R. M., Russo, N., Boelens, R., Kaptein, R., and van Boom, J. H. (1983) Sequential resonance assignments in DNA proton NMR spectra by two-dimensional NOE spectroscopy. *J. Am. Chem. Soc. 105*, 2914−2916.
(35) Macke, T. J., and Case, D. A. (1998) Modeling unusual nucleic acid structures. In *Molecular Modeling of Nucleic Acids* (Leontis, N. B., and SantaLucia, J., Eds.) pp 379−393, American Chemical Society, Washington, DC.
(36) Guéron, M., and Leroy, J. L. (1995) Studies of base pair kinetics by NMR measurement of proton exchange. *Methods Enzymol. 261*, 383−413.
(37) Plateau, P., and Guéron, M. (1982) Exchangeable proton NMR without base-line distortion, using new strong-pulse sequences. *J. Am. Chem. Soc. 104*, 7310−7311.
(38) Morris, G.A., and Freeman, R. (1978) Selective excitation in Fourier transform Nuclear Magnetic Resonance. *J. Magn. Reson. 29*, 433−462.
(39) Sikorski, W. H., Sanders, A. W., and Reich, H. J. (1998) Tris(trimethylsilyl)methane as an internal ^{13}C NMR chemical shift thermometer. *Magn. Reson. Chem. 36*, S118−S124.
(40) Raiford, D., Fisk, C., and Becker, E. D. (1979) Calibration of methanol and ethylene glycol nuclear magnetic resonance thermometers. *Anal. Chem. 51*, 2050−2051.
(41) Guéron, M., Charretier, E., Hagerhorst, J., Kochoyan, M., Leroy, J. L., and Moraillon, A. (1990) Applications of imino proton exchange to nucleic acid kinetics and structures. In *Structure and Methods Volume 3: DNA & RNA. Proceedings of the Sixth Conversation in the Discipline of Biomolecular Stereodynamics Held at the State University of New York at Albany, June 6−10, 1989* (Sarma, R. H., and Sarma, M. H., Eds.) Adenine Press, Schenectady, NY.
(42) Every, A. E., and Russu, I. M. (2008) Influence of magnesium ions on spontaneous opening of DNA base pairs. *J. Phys. Chem. B 112*, 7689−7695.
(43) Gray, D. M., Ratliff, R. L., and Vaughan, M. R. (1992) Circular dichroism spectroscopy of DNA. *Methods Enzymol. 211*, 389−406.
(44) Bush, C. A. (1974) Ultraviolet spectroscopy, circular dichroism, and optical rotatory dispersion. In *Basic Principles in Nucleic Acid Chemistry*, Academic Press, New York.
(45) Kypr, J., Kejnovska, I., Renciuk, D., and Vorlickova, M. (2009) Circular dichroism and conformational polymorphism in DNA. *Nucleic Acids Res. 37*, 1713−1725.
(46) Jackson, B.A., Alekseyev, V. Y., and Barton, J. K. (1999) A versatile mismatch recognition agent: Specific cleavage of a plasmid DNA at a single mispair. *Biochemistry 38*, 4655−4662.
(47) Jackson, B. J., and Barton, J. K. (2000) Recognition of base mismatches in DNA by 5,6-chrysenequinone diimine complexes of rhodium(III): A proposed mechanism for preferential binding to destabilized regions of the double helix. *Biochemistry 39*, 6176−6182.
(48) Guéron, M., Kochoyan, M., and Leroy, J. L. (1987) A single mode of DNA base-pair opening drives imino proton exchange. *Nature 328*, 89−92.
(49) Every, A. E., and Russu, I. M. (2007) Probing the role of hydrogen bonds in the stability of base pairs in double-helical DNA. *Biopolymers 87*, 165−173.
(50) Folta-Stogniew, E., and Russu, I. M. (1996) Base-catalysis of imino proton exchange in DNA: Effects of catalyst upon DNA structure and dynamics. *Biochemistry 35*, 8439−8449.
(51) Helbock, H., Beckman, K. B., Shigenaga, M. K., Walter, P., Woodall, A., Yeo, H., and Ames, B. (1998) DNA oxidation matters: The HPLC-electochemical detection assay of 8-oxo-deoxyguanosine and 8-oxo-guanine. *Proc. Natl. Acad. Sci. U.S.A. 95*, 288−293.
(52) Barone, F., Cellai, L., Giordano, C., Matzeu, M., Mazzei, F., and Pedone, F. (2000) γ-Ray footprinting and fluorescence polarization anisotropy of a 30-mer synthetic DNA fragment with one 2′-deoxy-7-hydro-8-oxoguanosine lesion. *Eur. Biophys. J. 28*, 621−628.

(53) Chinyengetere, F., and Jamieson, E. R. (2008) Impact of the oxidized guanine lesion spiroiminodihydantoin on the conformation and thermodynamic stability of a 15-mer DNA duplex. *Biochemistry 47*, 2584−2591.
(54) Bloomfield, V., Crothers, D., and Tinoco, I. (2000) *Nucleic Acids: Structures, Properties, and Functions*, University Science Books, Sausalito, CA.
(55) Markus, T. Z., Daube, S. S., Naaman, R., Fleming, A., Muller, J. G., and Burrows, C. J. (2009) Electronic structure of DNA-unique properties of 8-oxoguanosine. *J. Am. Chem. Soc. 131*, 89−95.
(56) Yavin, E., Stemp, E. D. A., O'Shea, V., David, S. S., and Barton, J. K. (2006) Electron trap for DNA-bound repair enzymes: A strategy for DNA-mediated signaling. *Proc. Natl. Acad. Sci. U.S.A. 103*, 3610−3614.
(57) Priyakumar, U. D., and MacKerell, A. (2006) Computational approaches for investigating base flipping in oligonucleotides. *Chem. Rev. 106*, 489−505.
(58) Priyakumar, U. D., and MacKerell, A. (2006) NMR imino proton exchange experiments on duplex DNA primarily monitor the opening of purine bases. *J. Am. Chem. Soc. 128*, 678−679.
(59) Spies, M. A., and Schowen, R. L. (2002) The trapping of a spontaneously "flipped out" base from double helical nucleic acids by host-guest complexation with β-cyclodextrin: The intrinsic base-flipping rate constant for DNA and RNA. *J. Am. Chem. Soc. 124*, 14049−14053.
(60) Brauns, E. B., Madaras, M. L., Coleman, R. S., Murphy, C. J., and Berg, M. (2002) Complex local dynamics in DNA on the picosecond and nanosecond timescales. *Phys. Rev. Lett. 88*, 158101−158104.
(61) Robinson, B. H., Mailer, C., and Drobny, G. (1997) Site-specific dynamics in DNA: Experiments. *Annu. Rev. Biophys. Biomol. Struct. 26*, 629−658.
(62) Marathias, V. M., Jerkovic, B., Arthanari, H., and Bolton, P. H. (2000) Flexibility and curvature of duplex DNA containing mismatched sites as a function of temperature. *Biochemistry 39*, 153−160.
(63) Singh, S., Szulik, M., Ganguly, M., Khutsishvilli, I., Stone, M., Marky, L., and Gold, B. (2011) Characterization of DNA with an 8-oxoguanine modification. *Nucleic Acids Res. 39*, 6789−6801.
(64) Blainey, P., van Oijen, A. M., Banerjee, A., Verdine, G. L., and Xie, X. S. (2006) A base-excision DNA-repair protein finds intrahelical lesion bases by fast sliding in contact with DNA. *Proc. Natl. Acad. Sci. U.S.A. 103*, 5752−5757.
(65) Stivers, J.T., and Jiang, Y. (2003) A mechanistic perspective on the chemistry of DNA repair glycosylases. *Chem. Rev. 103*, 2729−2759.
(66) David, S. S., and Williams, S. D. (1998) Chemistry of glycosylases and endonucleases involved in base-excision repair. *Chem. Rev. 98*, 1221−1261.